



Photodissociation of small group-14 atomic clusters in a multi-reflection time-of-flight mass spectrometer

Paul Fischer^a , Paul F. Giesel, and Lutz Schweikhard

Institut für Physik, Universität Greifswald, 17487 Greifswald, Germany

Received 29 November 2022 / Accepted 31 January 2023 / Published online 19 February 2023
© The Author(s) 2023

Abstract. Cationic and anionic clusters of the group-14 elements carbon, silicon, germanium, tin, and lead are produced by high-vacuum laser ablation and studied with a multi-reflection time-of-flight mass spectrometer. In-trap photodissociation is performed for cluster species in the size range $n = 2$ –10. The clusters' production rates as well as their dissociation pathways are used to probe the nonmetal–metal transition throughout the group. Carbon clusters show neutral-trimer break-off, while those of the other elements evaporate neutral monomers and, in some cases, form specific charged fragment sizes.

1 Introduction

An element's chemical and physical behavior can be reasonably inferred from its location in the periodic table. Not coincidentally, elements are grouped according to their valence electrons—the actors behind a number of fundamental properties. Comparing same-group elements will then reveal more complex trends arising from, for example, changes in the atomic radius.

Group 14 (IV) of the periodic table is notable for incorporating nonmetals (carbon), metalloids (silicon and germanium), and metals (tin and lead) [1]. While carbon forms strong, directional bonds, the bonding becomes weaker and less localized for the heavier elements and leads to metallization in the bulk.

Monoatomic clusters X_n —aggregates formed of n atoms of the same element X —allow the study of such trends with respect to their size: Growing from single atoms toward the bulk, atomic clusters probe the onset of properties associated with covalent or metallic bonding. Ion mobility measurements show, for example, that gas-phase lead clusters adopt the compact, near-spherical structures expected for metals [2], while carbon clusters exhibit more open geometries such as rings or chains [3]. Clusters of silicon, germanium, and—unexpectedly—tin only rearrange to spherical morphology above certain threshold sizes [4–6]. In other words, an element's bulk metallicity does not always translate to its small clusters in this region of the periodic table.

Naturally, the group has been the focus of much theoretical and experimental work; however, photodissociation has not yet been investigated for all species. Carbon cluster cations and anions have been extensively

studied [7–12] as have the cations of silicon [13–15]. Silicon and germanium cluster anions have been studied for $n \geq 9$ [16] and germanium cations for $n \geq 10$ [14]. For tin, photodissociation has only been performed with cluster anions starting from $n = 9$ [17], and for lead, investigations start from $n = 6$ for cations and $n = 9$ for anions [18]. Although fragmentation was also observed in photoionization studies, no precursor-resolved dissociation spectra were obtained [19, 20].

Here, the production rates, photodissociation pathways, and (in the case of anions) electron detachment of group-14 clusters from $n = 2$ to 10 are systematically investigated. Comparing elements, cluster sizes, and charge signs allows inferring the types of interatomic bonds and, thus, highlights the changing behavior throughout the group. The present results are gained from a single experimental setup under identical conditions, allowing direct comparisons.

A multi-reflection time-of-flight (MR-ToF) mass spectrometer, also known as an electrostatic ion beam trap (EIBT) [21, 22], is used for both precursor selection and fragment analysis. The device is capable of storing ions for extended periods of time by capturing them between two electrostatic mirrors. Long flight times and continuous temporal refocusing of the ion bunch by the reflecting potentials lead to mass resolving powers beyond 10^5 [23].

2 Experimental setup and procedure

The present setup (Fig. 1) consists of a high-vacuum laser-ablation source for cluster production ($\lambda = 532$ nm, 10 ns pulse width, 2 mm diameter on target), and a multi-reflection time-of-flight analyzer. The pulse

^a e-mail: paul.fischer@uni-greifswald.de (corresponding author)

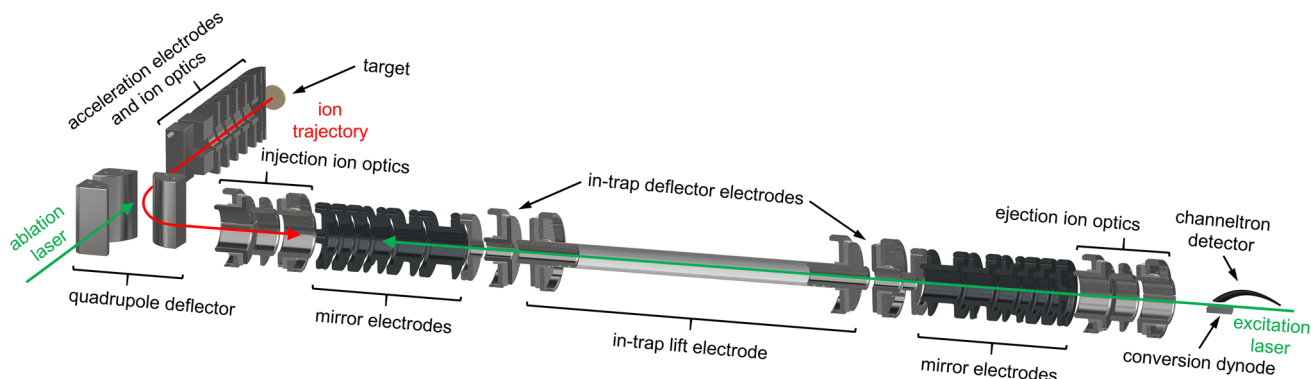


Fig. 1 Experimental setup for in-trap photoexcitation. Ions are produced by laser ablation from a target, excited by a second laser during storage, and detected after release from the trap

energy of the ablation laser is adjusted based on the target material (see Sect. 3). The target plates are biased to ± 2 kV to extract ions of either polarity and guide them in-between the electrostatic mirrors. The ions are either allowed to traverse the analyzer toward a channeltron ion detector for recording a conventional, linear time-of-flight spectrum (“single-path spectrum”), or their kinetic energy is reduced by an in-trap lift for capture [24].

Trapped ions revolve between the mirror potentials with distinct periods governed by their mass-to-charge ratios. The analyzer is equipped with in-trap deflector electrodes located between the mirrors and in-trap lift (see Fig. 1) for the application of radially deflecting electric fields during ion storage [25]. Synchronizing the switching of the deflector potentials to the revolution period of an ion species of interest allows the selection of specific mass numbers from a set of isotopologues, i.e., molecules with different isotopic compositions. The resolving and selection of Sn_5 isotopologues is exemplified in [25].

To probe the fragmentation of mass-selected clusters with the setup, an in-trap photodissociation technique has been developed [26]. Briefly, the molecular ion species of interest is captured and separated from contaminants in the MR-ToF analyzer over a few hundred revolutions. This is shown for a Sn_5^+ precursor and a storage duration of 500 periods in Fig. 2a, b. A pulsed excitation laser ($\lambda = 532$ nm, 6 ns pulse width, ≈ 3 mm diameter at point of interaction, 1 mJ pulse energy) is timed to excite the ions at their turn-around point in the entry-side ion mirror. Dissociation happening on short timescales ($\tau \lesssim 1 \mu\text{s}$), i.e., with the kinetic energy of the precursor close to zero, leads to the fragments leaving the mirror with identical total energies as the precursor. In the present study, all fragments are released toward the detector without further (multi-)reflection by switching off the exit-side mirror potential, yielding a time-of-flight product spectrum as shown in Fig. 2c.

The residual gas pressure in the MR-ToF analyzer is approximately 1×10^{-9} hPa. No collision-induced dissociation is observed for the present conditions, and nei-

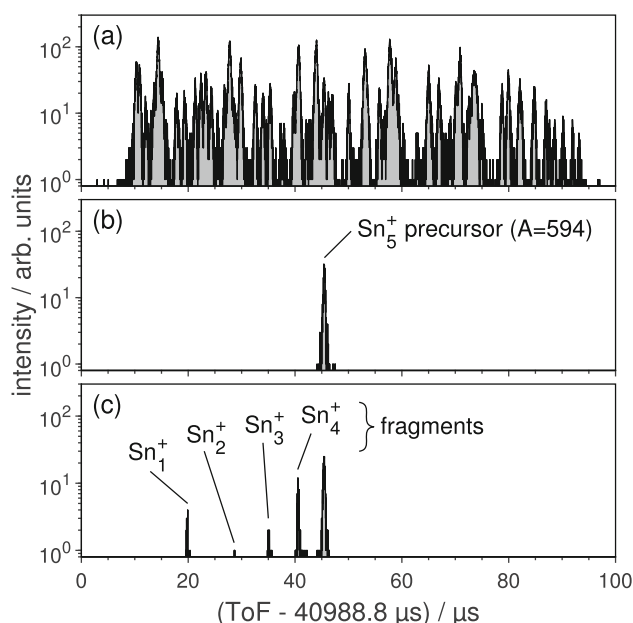


Fig. 2 ToF spectra after 500 Sn_5^+ revolutions to illustrate measurement scheme: **a** transversal ejection and photoexcitation disabled. **b** Transversal ejection enabled. **c** Transversal ejection and photoexcitation enabled

ther is unimolecular decay without prior photoexcitation.

3 Cluster production rates

The relative rates of the clusters' production by laser ablation give hints concerning their stability. This is investigated by recording single-path spectra for carbon, silicon, germanium, tin, and lead targets of 99.9% purity or above. Figure 3 gives an overview for all cationic and anionic cluster ions. For these measurements, the ablation-laser pulse energy (Table 1) and duration of data collection are adjusted between the species as the overall production yield varies. Figure 4

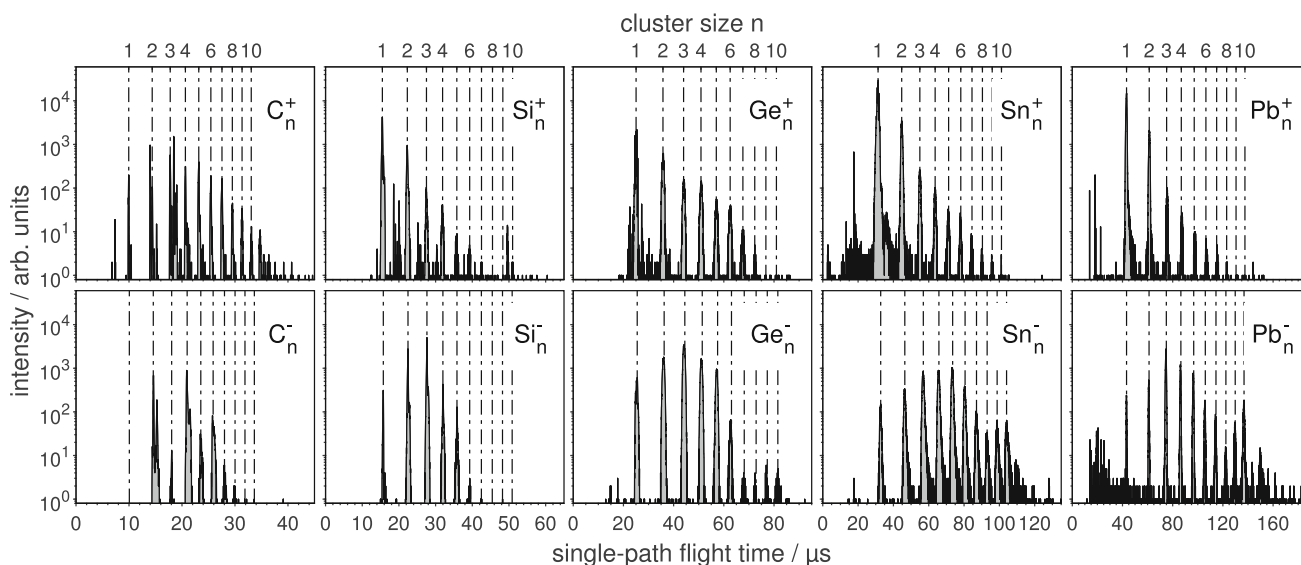


Fig. 3 Single-path time-of-flight spectra of group-14 cluster cations and anions produced by laser ablation of solid targets. Cluster sizes are marked by vertical lines

Table 1 Ablation-laser pulse energy in millijoule for group-14 cation and anion single-path spectra shown in Fig. 3

	C	Si	Ge	Sn	Pb
Cations	1.7	2.7	2.7	1.7	1.4
Anions	3.0	5.4	4.6	1.6	1.7

shows the detection rates per laser pulse extracted from the data. Note that systematic variations of the ablation-laser pulse energy are beyond the scope of the present study. While the general size range of produced clusters is typically only weakly affected by the pulse energy, the fact that spectra are recorded under different conditions has to be kept in mind when making quantitative comparisons.

As is known for laser ablation without aggregation gas, the observed cluster sizes are small since condensation via three-body collision is rare in the plume of vaporized material [27]. Thus, an overarching trend of (generally) decreasing abundance with cluster size is found. Beyond this phenomenon, however, fluctuations between neighboring sizes can reveal species with increased or decreased stability.

A notable exception, however, is the case of carbon-cluster cations C_n^+ which are produced from glassy carbon in the present study (Sigradur G, HTW Hochtemperatur-Werkstoffe GmbH): In addition to the small carbon clusters reported here, we recently observed large fullerenes with sizes up to $n \approx 800$ formed by coalescent growth from the laser-ablation source [28]. Such findings are in line with previous studies [29] and are linked to the specific structure of glassy carbon and, indeed, the nature of the carbon fullerenes themselves. This is, however, a very exceptional case,

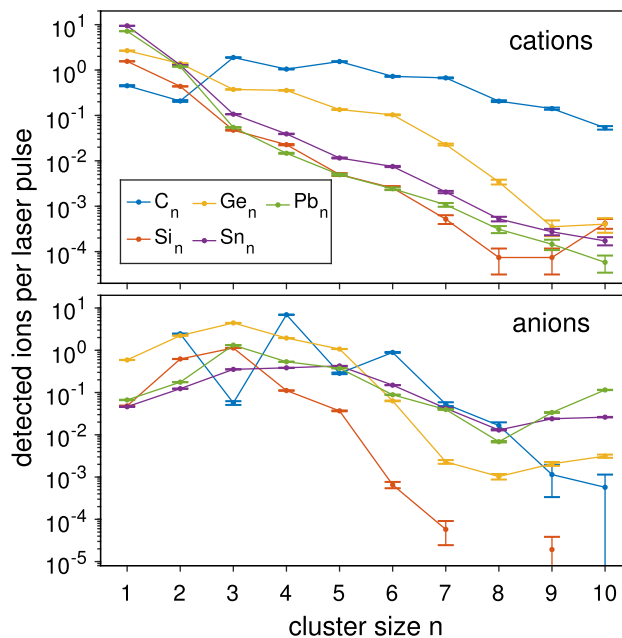


Fig. 4 Detected ion counts per ablation-laser pulse extracted from the spectra shown in Fig. 3. Note that no counts are observed for the C_1^- , Si_8^- , and Si_{10}^+ species and only a single count is for Si_9^- and C_{10}^- in these spectra

as discussed already in Ref. [28]. Thus, this feature will not be considered further in the present work.

The cationic cluster spectra for Si_n^+ , Ge_n^+ , Sn_n^+ , and Pb_n^+ (top row of Fig. 3 and top of Fig. 4) follow near-exponential abundance decreases with their cluster sizes—implying monomer aggregation [30]—with the largest observed size being $n \approx 10$. Carbon cations C_n^+ , while following the same decrease in general, show reduced abundance of the small sizes $n = 1-4$. Possibly,

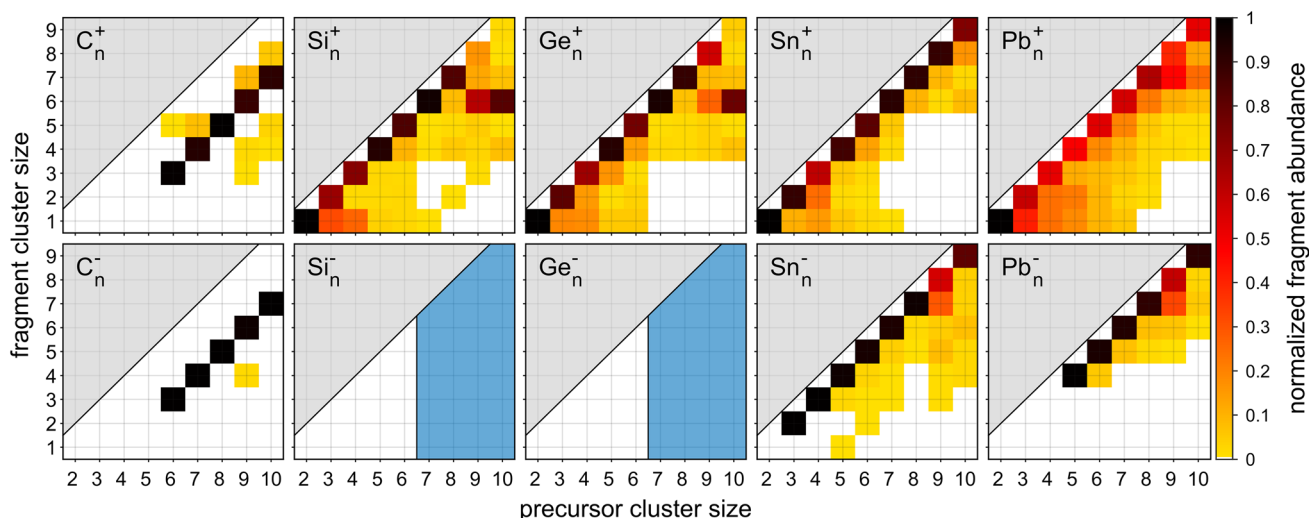


Fig. 5 Color-coded fragment abundances as a function of fragment size (y-axis) for group-14 cluster cations and anions after photoexcitation. Data are extracted from fragmentation spectra akin to Fig. 2c and normalized to the sum of all fragments for each precursor cluster. Each column adds up to one. Species for which no measurement could be performed due to low production are marked in blue. Empty columns indicate no fragments are observed

this is due to the coalescence mentioned above which may de-populate smaller species in favor of larger ones.

Similarly, the anion spectra of Si_n^- and the higher-period elements also resemble one another (bottom row of Fig. 3 and bottom of Fig. 4): The highest abundance is found at or around $n = 3$, and production strongly decreases after $n = 5$. The decrease in intensity becomes less prominent from Si_n^- to Pb_n^- . For Sn_n^- , Pb_n^- , and, to some extent, Ge_n^- , a second increase from $n = 8$ to $n = 10$ is found. The carbon spectrum is, again, markedly different: The production is dominated by a strong preference of the even-sized clusters over the odd-sized ones, and the atomic anion is not observed at all.

Signals not belonging to the combs of cluster sizes in Fig. 3 result from contaminants present in/on the targets or in the vacuum system. Signals can typically be matched to Na^+ or K^+ atoms or (compound) clusters for cationic and O^- or Cl^- for anionic species.

4 Cluster dissociation

It is known that even small metal clusters exhibit broad photoabsorption resonances through collective electronic excitations [31–33]. The absorbed energy can thermalize to the ro-vibrational system from where it is available for dissociation. In the present study, photoexcitation is always performed with photons of 2.33 eV (532 nm) and pulses of 1 mJ, leading to fragmentation of all of the probed cations except C_n^+ below $n = 6$. For the anionic species, electron detachment is dominant; however, some fragmentation is observed as well.

Figure 5 gives an overview of the dataset: Precursors between $n = 2$ and 10 are selected (horizontal axis), and the relative abundances of fragment sizes

are color-coded. A horizontal trend of darker colors in the map shows preference for a specific fragment being formed across multiple precursors (e.g., Si_6^+). A diagonal trend signals the loss of identical neutral fragments from different precursors (e.g., C_3 , forming C_{n-3}^\pm). Multiple darker squares in a single column indicate different fragment sizes being formed with similar abundances from a single precursor (e.g., Sn_7^- and Sn_8^- from Sn_9^-). Electron-detachment rates are obtained from the difference in total signal between fragment and reference spectra.

The amount of loss of neutral fragments as a function of cluster size is further illustrated for cations (Fig. 6) and anions (Fig. 7), respectively. For each precursor of size n , the relative abundances for the $(n - 1)$ through $(n - 4)$ charged species are plotted, correlating to the loss of 1, 2, 3, or 4 neutral atoms. Whether these losses occur sequentially or by break-off of larger pieces cannot be determined directly from the present data but will be further discussed below.

4.1 Neutral C_3 break-off

The loss of neutral C_3 fragments from small carbon-cluster cations and anions is well documented [7–12] and found to be the dominant decay channel for $n \geq 6$ in the present study as well (Fig. 5 and blue lines in Figs. 6, 7). While the anion decay pathways show no branching, i.e., (virtually) 100% of the fragments are found in the $(n - 3)$ signal, the cations show $(n - 2)$ abundances of up to $\approx 10\%$. Isomer-resolved dissociation studies have shown high amounts of C_3 loss to be indicative of a linear cluster geometry, while larger portions of C_2 loss point to a cyclic geometry [34, 35]. Thus, it may be possible that cyclic isomers are more readily produced for the cationic species in the present study.

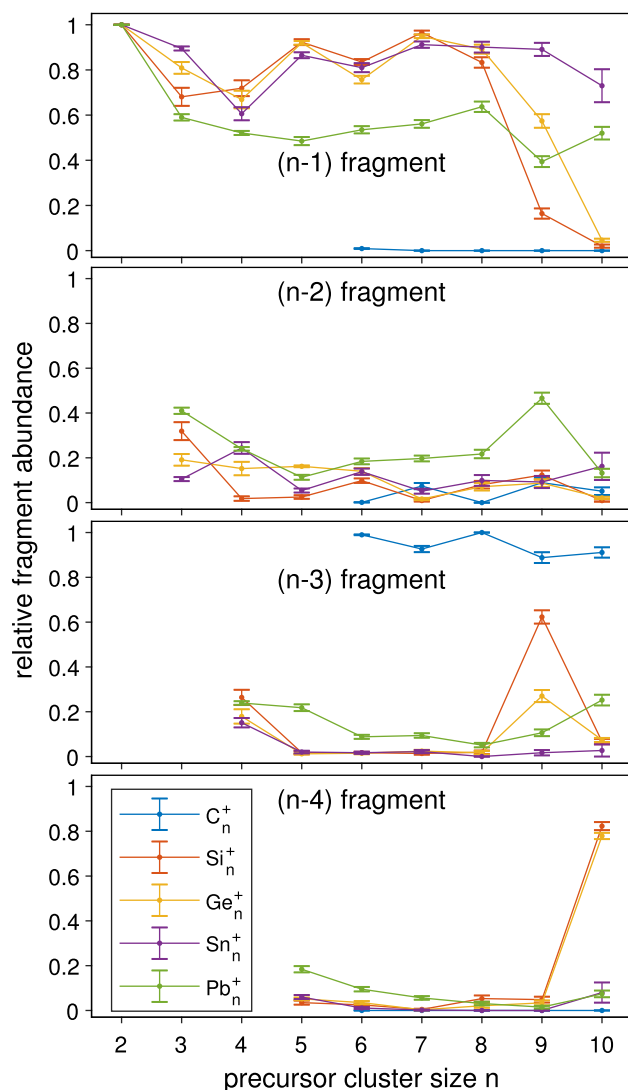


Fig. 6 Relative abundances of $(n-1)$ to $(n-4)$ fragments with respect to all observed fragments for cation precursors up to $n = 10$. Data are only plotted from $n = 6$ onward for carbon due to lack of fragmentation below

In any case, the fragmentation patterns demonstrate the covalent bonding of carbon molecules and show—as expected—no indication of metallic behavior.

4.2 Evaporation of neutral monomers

In contrast to those with covalent bonds, clusters with predominantly metallic bonding are more likely to evaporate single neutral atoms. This is most prominently known for alkali and coinage metals [36,37] which are exemplary metal clusters due to their strongly delocalized s electrons. Note that the s^1 configuration of those elements specifically also leads to neutral-dimer break-off from small odd-sized mono-cations to satisfy electron pairing [37,38].

In the present study, monomer loss is found as a dominant channel for many precursors of Si^+ , Ge^+ ,

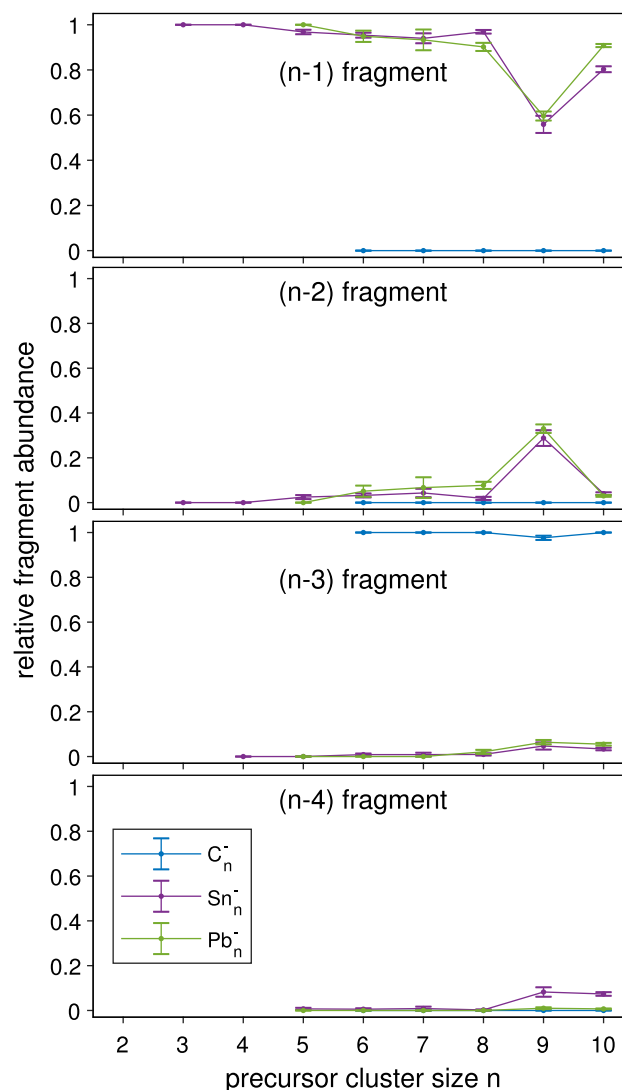


Fig. 7 Relative abundances of $(n-1)$ to $(n-4)$ fragments for anion precursors up to $n = 10$. Data are only plotted from $n = 6, 3,$ and 5 onward for carbon, tin, and lead, respectively, due to lack of fragmentation below. No fragmentation has been observed for any silicon or germanium cluster anions

Sn^\pm , and Pb^\pm . A metal-type bond can, however, not directly be concluded at these small cluster sizes. It is known that larger clusters of silicon and germanium will adopt different dissociation patterns [14], as can already be seen for $n \geq 9$ in Figs. 5 and 6. Tin [17] and lead [18] clusters of intermediate sizes will lose larger neutral fragments in competition with monomers.

Nonetheless, it is noteworthy that the small lead cations observed in the present study—which, to our knowledge, have not been previously probed by photoexcitation—show a much stronger preference for *sequential* loss of multiple atoms compared to tin and the other elements. More product cluster sizes are observed in higher abundance in Fig. 5, and in Fig. 6, the green $(n-1)$ line is actually reduced in favor of

the $(n - 2)$ and $(n - 3)$ lines. This highlights the merit of comparing data recorded under identical experimental conditions for multiple elements and supports the narrative that the covalent bonding in lead clusters is yet weaker than for tin and, by extension, the group's lighter elements.

4.3 Formation of specific fragments

Si_6^+ and Ge_6^+

Silicon cations of size $n = 9$ and 10 are found to predominantly lose larger neutral fragments to form Si_6^+ (Fig. 5 and spikes in yellow and orange $(n - 3)$ and $(n - 4)$ lines in Fig. 6). This is in agreement with previous studies for 532-nm photodissociation [13] and collision-induced dissociation [39] as well as ab initio calculations [40]. For 355-nm photodissociation, monomer evaporation has been found as the dominant channel for $n = 9$ [15].

Similarities between silicon and germanium clusters have been noted before [14, 41, 42]. In the present study, larger germanium cations show the same preference as silicon to form charged fragments with size $n = 6$. In fact, the dissociation patterns of the two elements are remarkably similar—and markedly different from those of the nonmetal carbon and the metals tin and lead. In other words, while the metalloids of group 14 might not adopt the compact structures of the metal clusters, they are more closed than the linear chains or rings of carbon.

Sn_7^- and Pb_7^-

Similarly to the above considerations, anionic tin and lead precursors of size $n = 9$ —but not 10—form charged $n = 7$ fragments (spikes in purple and green $(n - 2)$ lines in Fig. 7). Both observations are explained by an increased stability of the tin and lead heptamers and decamers due to favorable geometries [43–48].

Remarkably, while the cation Pb_9^+ shows the same preference to form the charged $n = 7$ fragment as a competing dissociation channel to the sequential monomer loss (spike in green $(n - 2)$ line in Fig. 6), Sn_9^+ does not. More generally speaking, the dissociation maps in Fig. 5 resemble each other for the anionic tin and lead clusters but not the cationic ones.

Note that there are indications for enhanced heptamer and decamer stability also in the Sn_n^- and Pb_n^- single-path spectra (Fig. 3): Abundance drops occur after $n = 7$ and $n = 10$ in both cases. Interestingly, a similar effect is visible for the Ge_n^- and, possibly, the Si_n^- spectrum. While no photofragments have been observed for silicon and germanium cluster anions in the present study due to dominant electron detachment for $n \leq 6$ (see Sect. 4.5) and lack of production for $n > 6$, their dissociation pathways may well show similarities to tin and lead.

4.4 Formation of the monomer cation

It is noticeable in Fig. 5 that clusters of Si_n^+ , Ge_n^+ , Sn_n^+ , and Pb_n^+ with $n \lesssim 6$ show some preference to form their respective charged monomer species. This is also exemplified in the dissociation spectrum of Sn_5^+ in Fig. 2c. To our knowledge, this trend has not been previously reported for these species, whereas it is known from dissociation patterns of, for example, aluminum clusters [49–51]. In that case, it is linked to the fact that small Al clusters have—opposed to most other metallic clusters—larger ionization potentials than the atom. This is true for some but not all species in question here [52–54].

However, it can also be argued that sequential monomer evaporation of small cationic clusters has to inevitably terminate with the atomic ion. While it cannot be ruled out that (part of) the phenomenon may have to be accredited to this, variations of the excitation-laser pulse energy E_p are performed for precursors Ge_5^+ , Sn_5^+ , and Pb_5^+ for more clarity. Figure 8 illustrates the results for Ge_5^+ ; the two other cases show similar behavior.

Firstly, the $(n - 1)$ fragment, Ge_4^+ , follows a linear dependence with the pulse energy. This supports the assumption that neutral-monomer loss is the lowest dissociation channel as it is attained by single-photon absorption. The Ge_3^+ and Ge_2^+ curves are best described by cubic functions, implying three-photon absorption and, thus, higher threshold energies for the dissociation processes. The Ge_1^+ dependence is only fully characterized by superposition of a linear and higher-order term (see dashed lines in Fig. 8 for the individual components).

While the exponent of the second term cannot be unambiguously concluded due to the limited number of data points, the use of a cubic function reproduces the measurement well. Note that the binding energy per atom is on the order of 2–3 eV for small germanium clusters [55], so two-photon absorption might be more likely. In any case, it is reasonable to propose that the Ge_1^+ fragment is produced through multiple pathways: The linear component should result from monomer loss of Ge_5^+ with the monomer retaining the charge, i.e.,



The higher-order component could result from one or more of the subsequent reactions



after an initial loss of neutral mono- and/or di- or trimers. This in turn implies that at least two reactions exhibit a degeneracy with respect to which species retains the charge.

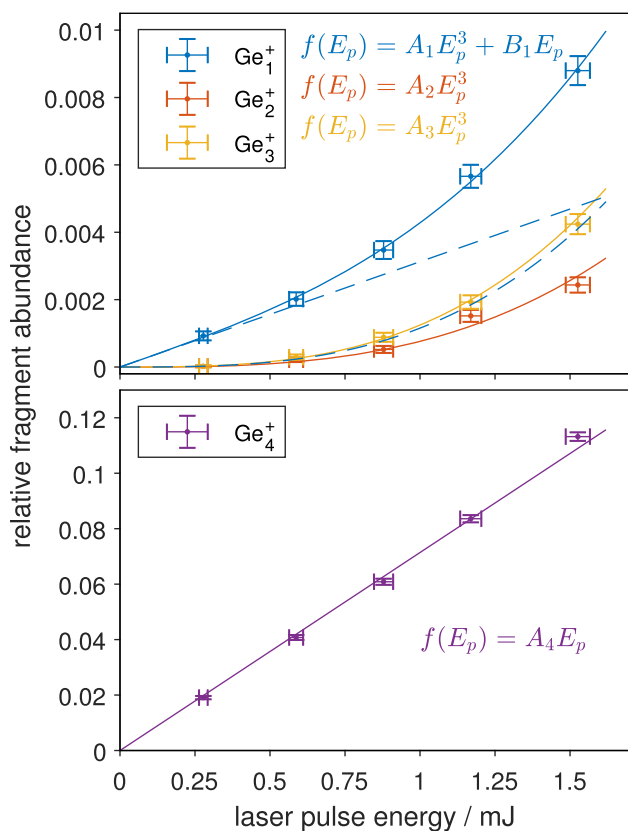


Fig. 8 Fragment abundances from photoexcitation of Ge_5^+ as a function of excitation-laser pulse energy. Polynomials are fitted to the data (solid lines) as indicated by the labels. The dashed lines show the linear and cubic components of the Ge_1^+ trend

Note that the scaling factors A_1 and A_3 (see Fig. 8) for the cubic functions describing the Ge_1^+ and Ge_3^+ abundances are virtually identical, which, however, does not allow further conclusions due to the number of possible reaction pathways. Also, note that clusters produced with the present laser-ablation source are not thermalized to room temperature due to the absence of aggregation gas [56]. This suggests broad distributions of the clusters' ro-vibrational energies even prior to the excitation and, thus, matches the findings of degenerate dissociation channels.

4.5 Overall reactivity and electron detachment

In addition to the size-resolved fragment spectra above, information can be obtained from the overall dissociation or, in case of anions, electron-detachment yields (Fig. 9). For the cations, in general, more fragmentation is observed going from carbon to lead, which may be linked to the trend of the clusters' bonds becoming less covalent.

A striking feature is the strong oscillation of fragmentation abundance between Sn_2^+ and Sn_6^+ , which correlates well with the trend in calculated fragmentation energies [45]. The same oscillations can be seen for sil-

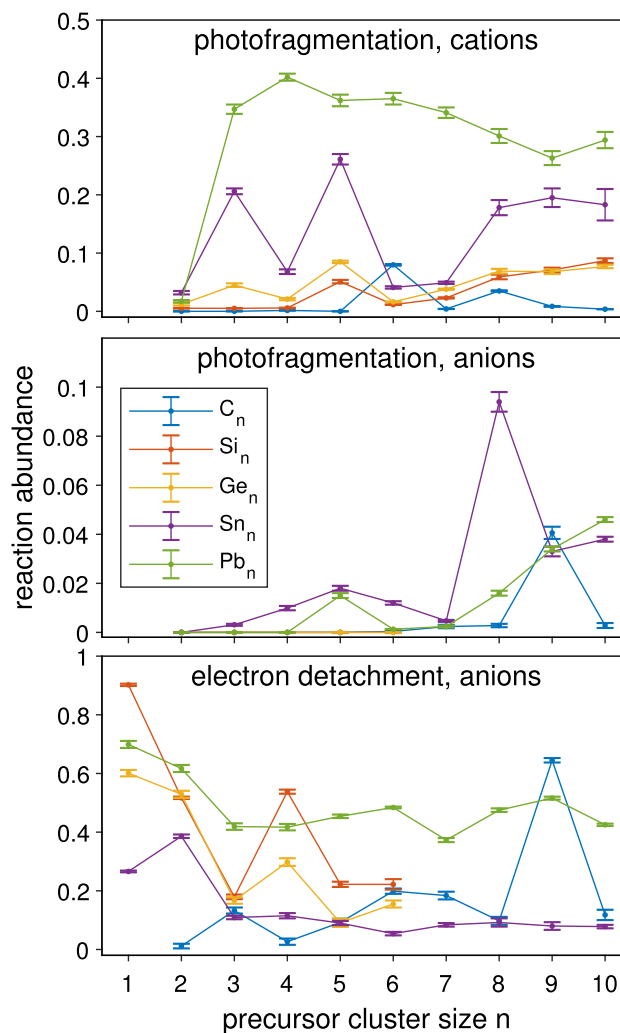


Fig. 9 Relative abundance of all photofragments and missing signal due to electron detachment in the case of anions. All data are normalized to the precursor abundance before photoexcitation. No measurements were performed for C_1^- as well as Si_n^- and Ge_n^- for $n = 7-10$ due to insufficient production rates

icon and germanium cations, the calculated energies of which also show staggering [57]. The fragmentation energies of lead cations vary less and are also much lower in general [48].

For the anionic clusters, electron detachment is generally prevalent over dissociation. This effect is strongest for silicon and germanium: No fragmentation is observed at all for $n \leq 6$, and production is too low for photoexcitation above. Possibly, this follows from electron detachment already being very likely for the larger clusters in the hot plume during laser ablation. Interestingly, while the measured electron affinities of Si_n^- and Ge_n^- are below the photon energy in this size range [58], those of Sn_n^- and Pb_n^- are comparable, if not lower [59]. This is taken as another confirmation of the more metallic character of the lead and tin clusters: The collective resonances known to exist for the elec-

tron gas of metal clusters [31–33] might allow photons to be absorbed and their energy to be thermalized to the ro-vibrational system without electron detachment.

A notable feature in the trend of anionic cluster fragmentation is the strong spike observed for Sn_8^- . This can be linked, again, to the favorable geometry of the $n = 7$ cluster. The ground-state structure of the octamer is closely related to that of the heptamer; consequently, its fragmentation energy is significantly reduced [44]. Interestingly, although the preference for dimer break-off from Pb_9^- implies the same stability of the $n = 7$ lead cluster, no increased fragmentation abundance is observed for Pb_8^- .

Both the detachment and fragmentation abundances spike for C_9^- for which no obvious reason could be found. While this may be a similar effect as the one observed for tin and lead, i.e., forming preferable fragment configurations, the detachment and dissociation channels would result in different product clusters.

5 Summary and conclusion

The photodissociation pathways of group-14 cluster cations and anions with sizes $n \leq 10$ are analyzed. The study completes earlier photoexcitation investigations across the group and also highlights the usefulness of data taken for multiple elements under comparable experimental conditions. Thus, the results offer a comparison that hints to the elements' preferences for covalent or metallic bonding in the corresponding small-sized atomic clusters.

Carbon stands alone as the group's only true non-metal. The remaining four elements' clusters all show some similarities, with none acting like true metals or nonmetals in all criteria. The silicon and germanium results are very comparable, as are those, to a lesser extend, of tin and lead. While lead cations Pb_n^+ show dissociation most akin to that expected for metal clusters—sequential evaporation of neutral monomers— Si_n^+ and Ge_n^+ also show a preference to form $n = 6$ charged fragments. Tin and lead anions Sn_n^- and Pb_n^- form $n = 7$ charged fragments, analogously, while only electron detachment is found for Si_n^- and Ge_n^- . Tin cationic clusters are somewhat particular in the sense that their dissociation channels match neither those of the lead nor the silicon/germanium cations fully. This confirms tin as the most inconsistent element with respect to the metal–nonmetal crossing among the already fickle group 14.

Author contributions

PF and LS conceived the experiment. PF and PFG performed the measurements and preliminary data evaluation. PF performed the final data analysis and prepared the first draft of the manuscript, which was edited by all authors.

Funding Information Open Access funding enabled and organized by Projekt DEAL.

Data Availability Statement This manuscript has no associated data, or the data will not be deposited. The datasets generated during and/or analyzed during the current study are available from the corresponding author on reasonable request.

Open Access This article is licensed under a Creative Commons Attribution 4.0 International License, which permits use, sharing, adaptation, distribution and reproduction in any medium or format, as long as you give appropriate credit to the original author(s) and the source, provide a link to the Creative Commons licence, and indicate if changes were made. The images or other third party material in this article are included in the article's Creative Commons licence, unless indicated otherwise in a credit line to the material. If material is not included in the article's Creative Commons licence and your intended use is not permitted by statutory regulation or exceeds the permitted use, you will need to obtain permission directly from the copyright holder. To view a copy of this licence, visit <http://creativecommons.org/licenses/by/4.0/>.

References

1. P. Atkins, T. Overton, J. Rourke, M. Weller, F. Armstrong, *Shriver and Atkins' Inorganic Chemistry*, 5th edn. (Oxford University Press, Oxford, 2010)
2. A.A. Shvartsburg, M.F. Jarrold, Transition from covalent to metallic behavior in group-14 clusters. *Chem. Phys. Lett.* **317**(6), 615–618 (2000). [https://doi.org/10.1016/S0009-2614\(99\)01416-5](https://doi.org/10.1016/S0009-2614(99)01416-5)
3. G. von Helden, M.T. Hsu, N. Gotts, M.T. Bowers, Carbon cluster cations with up to 84 atoms: structures, formation mechanism, and reactivity. *J. Phys. Chem.* **97**(31), 8182–8192 (1993). <https://doi.org/10.1021/j100133a011>
4. M.F. Jarrold, V.A. Constant, Silicon cluster ions: evidence for a structural transition. *Phys. Rev. Lett.* **67**, 2994–2997 (1991). <https://doi.org/10.1103/PhysRevLett.67.2994>
5. J.M. Hunter, J.L. Fye, M.F. Jarrold, J.E. Bower, Structural transitions in size-selected germanium cluster ions. *Phys. Rev. Lett.* **73**, 2063–2066 (1994). <https://doi.org/10.1103/PhysRevLett.73.2063>
6. A.A. Shvartsburg, M.F. Jarrold, Tin clusters adopt prolate geometries. *Phys. Rev. A* **60**, 1235–1239 (1999). <https://doi.org/10.1103/PhysRevA.60.1235>
7. M.E. Geusic, M.F. Jarrold, T.J. McIlrath, R.R. Freeman, W.L. Brown, Photodissociation of carbon cluster cations. *J. Chem. Phys.* **86**(7), 3862–3869 (1987). <https://doi.org/10.1063/1.451946>
8. R. Bouyer, F. Roussel, P. Monchicourt, M. Perdrix, P. Pradel, Energetics of C_{16}^+ to C_{36}^+ photodissociation. *J. Chem. Phys.* **100**(12), 8912–8919 (1994). <https://doi.org/10.1063/1.466695>
9. R. Bouyer, P. Monchicourt, M. Perdrix, P. Pradel, F. Roussel, Photodissociation kinetics of C_n^+ clusters. *J. Phys. B* **30**(1), 135 (1997). <https://doi.org/10.1088/0953-4075/30/1/015>

10. B.P. Pozniak, R.C. Dunbar, Photodissociation studies of C_n^+ at 193 nm ($n=5-19$). *Int. J. Mass Spectrom.* **165–166**, 299–313 (1997). [https://doi.org/10.1016/S0168-1176\(97\)00193-6](https://doi.org/10.1016/S0168-1176(97)00193-6)
11. M.J. Deluca, M.A. Johnson, Photofragmentation of C_n^- , $4 \leq n \leq 20$: loss of neutral C_3 . *Chem. Phys. Lett.* **152**(1), 67–70 (1988). [https://doi.org/10.1016/0009-2614\(88\)87329-9](https://doi.org/10.1016/0009-2614(88)87329-9)
12. B. Pozniak, R.C. Dunbar, Photodissociation and photodetachment of small carbon cluster anions. *Int. J. Mass Spectrom.* **133**(2), 97–110 (1994). [https://doi.org/10.1016/0168-1176\(94\)03963-1](https://doi.org/10.1016/0168-1176(94)03963-1)
13. L.A. Bloomfield, R.R. Freeman, W.L. Brown, Photofragmentation of mass-resolved Si_{2-12}^+ clusters. *Phys. Rev. Lett.* **54**, 2246–2249 (1985). <https://doi.org/10.1103/PhysRevLett.54.2246>
14. Q.-L. Zhang, Y. Liu, R.F. Curl, F.K. Tittel, R.E. Smalley, Photodissociation of semiconductor positive cluster ions. *J. Chem. Phys.* **88**(3), 1670–1677 (1988). <https://doi.org/10.1063/1.454145>
15. P. Ferrari, E. Janssens, P. Lievens, K. Hansen, Thermal radiation and fragmentation pathways of photo-excited silicon clusters. *J. Chem. Phys.* **143**(22), 224313 (2015). <https://doi.org/10.1063/1.4936917>
16. Y. Liu, Q.-L. Zhang, F.K. Tittel, R.F. Curl, R.E. Smalley, Photodetachment and photofragmentation studies of semiconductor cluster anions. *J. Chem. Phys.* **85**(12), 7434–7441 (1986). <https://doi.org/10.1063/1.451332>
17. M. Wolfram, S. Bandelow, A. Jankowski, S. König, G. Marx, L. Schweikhard, Photodissociation of mono- and di-anionic tin clusters. *Eur. Phys. J. D* **74**(6), 135 (2020). <https://doi.org/10.1140/epjd/e2020-100614-2>
18. S. König, F. Martinez, L. Schweikhard, M. Wolfram, Photodecay pathways of stored, size-selected lead clusters Pb_n^+ , $n=6-41$ and Pb_n^- , $n=9-56$. *J. Phys. Chem. C* **121**(20), 10858–10864 (2017). <https://doi.org/10.1021/acs.jpcc.6b12074>
19. K. LaiHing, R.G. Wheeler, W.L. Wilson, M.A. Duncan, Photoionization dynamics and abundance patterns in laser vaporized tin and lead clusters. *J. Chem. Phys.* **87**(6), 3401–3409 (1987). <https://doi.org/10.1063/1.452984>
20. R.W. Farley, P. Ziemann, A.W. Castleman, Investigation of the stabilities of neutral and ionic lead and lead-antimony clusters under single and multiphoton ionization conditions. *Z. Phys. D* **14**(4), 353–360 (1989). <https://doi.org/10.1007/BF01429285>
21. D. Zajfman, O. Heber, L. Vejby-Christensen, I. Ben-Itzhak, M. Rappaport, R. Fishman, M. Dahan, Electrostatic bottle for long-time storage of fast ion beams. *Phys. Rev. A* **55**, 1577–1580 (1997). <https://doi.org/10.1103/PhysRevA.55.R1577>
22. W.H. Benner, A gated electrostatic ion trap to repetitiously measure the charge and m/z of large electrospray ions. *Anal. Chem.* **69**(20), 4162–4168 (1997). <https://doi.org/10.1021/ac970163e>
23. P. Fischer, L. Schweikhard, Multiple active voltage stabilizations for multi-reflection time-of-flight mass spectrometry. *Rev. Sci. Instrum.* **92**(6), 063203 (2021). <https://doi.org/10.1063/5.0050568>
24. R.N. Wolf, G. Marx, M. Rosenbusch, L. Schweikhard, Static-mirror ion capture and time focusing for electrostatic ion-beam traps and multi-reflection time-of-flight mass analyzers by use of an in-trap potential lift. *Int. J. Mass Spectrom.* **313**, 8–14 (2012). <https://doi.org/10.1016/j.ijms.2011.12.006>
25. P. Fischer, S. Knauer, G. Marx, L. Schweikhard, In-depth study of in-trap high-resolution mass separation by transversal ion ejection from a multi-reflection time-of-flight device. *Rev. Sci. Instrum.* **89**(1), 015114 (2018). <https://doi.org/10.1063/1.5009167>
26. P. Fischer, L. Schweikhard, Photofragmentation of $Bi_n^{+/-}$ clusters ($n = 2-19$) in an electrostatic ion beam trap. *Eur. Phys. J. D* **73**(5), 105 (2019). <https://doi.org/10.1140/epjd/e2019-100027-0>
27. M.A. Duncan, Invited review article: laser vaporization cluster sources. *Rev. Sci. Instrum.* **83**(4), 041101 (2012). <https://doi.org/10.1063/1.3697599>
28. P. Fischer, L. Schweikhard, Disentangling poly-cationic fullerenes produced from glassy carbon with multi-reflection time-of-flight mass spectrometry (accepted). *Phys. Rev. Res.* (2022). <https://doi.org/10.1103/PhysRevResearch.4.043187>
29. J. Maul, T. Berg, E. Marosits, G. Schönhense, G. Huber, Statistical mechanics of fullerene coalescence growth. *Phys. Rev. B* **74**, 161406 (2006). <https://doi.org/10.1103/PhysRevB.74.161406>
30. J.A. Alonso, *Structure and Properties of Atomic Nanoclusters*, 2nd edn. (Imperial College Press, London, 2011)
31. V.V. Kresin, Collective resonances and response properties of electrons in metal clusters. *Phys. Rep.* **220**(1), 1–52 (1992). [https://doi.org/10.1016/0370-1573\(92\)90056-6](https://doi.org/10.1016/0370-1573(92)90056-6)
32. C. Bréchnignac, J.P. Connerade, Giant resonances in free atoms and in clusters. *J. Phys. B* **27**(17), 3795 (1994). <https://doi.org/10.1088/0953-4075/27/17/008>
33. I. Vasiliev, S. Ögüt, J.R. Chelikowsky, Ab initio excitation spectra and collective electronic response in atoms and clusters. *Phys. Rev. Lett.* **82**, 1919–1922 (1999). <https://doi.org/10.1103/PhysRevLett.82.1919>
34. F. Misaizu, N. Hori, H. Tanaka, K. Komatsu, A. Furuya, K. Ohno, Isomer-selected photoreactions of gas-phase cluster ions. *Eur. Phys. J. D* **52**(1), 59–62 (2009). <https://doi.org/10.1140/epjd/e2008-00268-x>
35. K. Koyasu, T. Ohtaki, N. Hori, F. Misaizu, Isomer-resolved dissociation of small carbon cluster cations, $C_7^+ - C_{10}^+$. *Chem. Phys. Lett.* **523**, 54–59 (2012). <https://doi.org/10.1016/j.cplett.2011.12.032>
36. C. Bréchnignac, P. Cahuzac, F. Carlier, M. de Frutos, J. Leygnier, Alkali-metal clusters as prototypes of metal clusters. *J. Chem. Soc. Faraday Trans.* **86**, 2525–2531 (1990). <https://doi.org/10.1039/FT9908602525>
37. M. Vogel, A. Herlert, L. Schweikhard, Photodissociation of small group-11 metal cluster ions: fragmentation pathways and photoabsorption cross sections. *J. Am. Soc. Mass Spectrom.* **14**(6), 614–621 (2003). [https://doi.org/10.1016/S1044-0305\(03\)00203-4](https://doi.org/10.1016/S1044-0305(03)00203-4)
38. S. Nonose, H. Tanaka, T. Mizuno, J. Hirokawa, T. Kondow, Role of electron pairing in collisional dissociation of Na_9^+ by a rare-gas atom. *J. Chem. Phys.* **104**(15), 5869–5874 (1996). <https://doi.org/10.1063/1.471318>
39. M.F. Jarrold, J.E. Bower, Collision-induced dissociation of silicon cluster ions. *J. Phys. Chem.* **92**(20), 5702–5705 (1988). <https://doi.org/10.1021/j100331a031>

40. K. Raghavachari, C.M. Rohlfing, Bonding and stabilities of small silicon clusters: a theoretical study of Si₇-Si₁₀. *J. Chem. Phys.* **89**(4), 2219–2234 (1988). <https://doi.org/10.1063/1.455065>
41. J.R. Heath, Y. Liu, S.C. O'Brien, Q.-L. Zhang, R.F. Curl, F.K. Tittel, R.E. Smalley, Semiconductor cluster beams: one and two color ionization studies of Si_x and Ge_x. *J. Chem. Phys.* **83**(11), 5520–5526 (1985). <https://doi.org/10.1063/1.449673>
42. G. Pacchioni, J. Koutecký, Silicon and germanium clusters. A theoretical study of their electronic structures and properties. *J. Chem. Phys.* **84**(6), 3301–3310 (1986). <https://doi.org/10.1063/1.450262>
43. B. Wang, L.M. Molina, M.J. López, A. Rubio, J.A. Alonso, M.J. Stott, Comparative ab initio studies of small tin and lead clusters. *Ann. Phys.* **510**(2), 107–119 (1998). <https://doi.org/10.1002/andp.19985100205>
44. E. Oger, R. Kelting, P. Weis, A. Lechtken, D. Schooss, N.R.M. Crawford, R. Ahlrichs, M.M. Kappes, Small tin cluster anions: transition from quasispherical to prolate structures. *J. Chem. Phys.* **130**(12), 124305 (2009). <https://doi.org/10.1063/1.3094320>
45. N. Drebov, E. Oger, T. Rapps, R. Kelting, D. Schooss, P. Weis, M.M. Kappes, R. Ahlrichs, Structures of tin cluster cations Sn₃⁺ to Sn₁₅⁺. *J. Chem. Phys.* **133**(22), 224302 (2010). <https://doi.org/10.1063/1.3514907>
46. B. Wang, J. Zhao, X. Chen, D. Shi, G. Wang, Atomic structures and covalent-to-metallic transition of lead clusters Pb_n (n=2-22). *Phys. Rev. A* **71**, 033201 (2005). <https://doi.org/10.1103/PhysRevA.71.033201>
47. C. Rajesh, C. Majumder, Atomic and electronic structures of neutral and charged Pb_n clusters (n=2-15): theoretical investigation based on density functional theory. *J. Chem. Phys.* **126**(24), 244704 (2007). <https://doi.org/10.1063/1.2741537>
48. R. Kelting, R. Otterstätter, P. Weis, N. Drebov, R. Ahlrichs, M.M. Kappes, Structures and energetics of small lead cluster ions. *J. Chem. Phys.* **134**(2), 024311 (2011). <https://doi.org/10.1063/1.3518040>
49. M.F. Jarrold, J.E. Bower, J.S. Kraus, Collision induced dissociation of metal cluster ions: bare aluminum clusters, Al_n⁺ (n=3-26). *J. Chem. Phys.* **86**(7), 3876–3885 (1987). <https://doi.org/10.1063/1.451948>
50. U. Ray, M.F. Jarrold, J.E. Bower, J.S. Kraus, Photodissociation spectroscopy of aluminum clusters: Al₃⁺-Al₆⁺. *Chem. Phys. Lett.* **159**(2), 221–226 (1989). [https://doi.org/10.1016/0009-2614\(89\)87413-5](https://doi.org/10.1016/0009-2614(89)87413-5)
51. U. Ray, M.F. Jarrold, J.E. Bower, J.S. Kraus, Photodissociation kinetics of aluminum cluster ions: determination of cluster dissociation energies. *J. Chem. Phys.* **91**(5), 2912–2921 (1989). <https://doi.org/10.1063/1.456961>
52. K. Fuke, K. Tsukamoto, F. Misaizu, M. Sanekata, Near threshold photoionization of silicon clusters in the 248–146 nm region: ionization potentials for Si_n. *J. Chem. Phys.* **99**(10), 7807–7812 (1993). <https://doi.org/10.1063/1.465658>
53. S. Yoshida, K. Fuke, Photoionization studies of germanium and tin clusters in the energy region of 50–88 eV: Ionization potentials for Ge_n (n=2-57) and Sn_n (n=2-41). *J. Chem. Phys.* **111**(9), 3880–3890 (1999). <https://doi.org/10.1063/1.479691>
54. Y. Saito, K. Yamauchi, K. Mihama, T. Noda, Formation and ionization potentials of lead clusters. *Jpn. J. Appl. Phys.* **21**(6A), 396 (1982). <https://doi.org/10.1143/JJAP.21.L396>
55. J. Wang, G. Wang, J. Zhao, Structure and electronic properties of ge_n (n = 2 – 25) clusters from density-functional theory. *Phys. Rev. B* **64**, 205411 (2001). <https://doi.org/10.1103/PhysRevB.64.205411>
56. P. Fischer, L. Schweikhard, Decay-rate power-law exponent as a link between dissociation energy and temperature. *Phys. Rev. Res.* **2**, 043177 (2020). <https://doi.org/10.1103/PhysRevResearch.2.043177>
57. A.A. Shvartsburg, B. Liu, Z.-Y. Lu, C.-Z. Wang, M.F. Jarrold, K.-M. Ho, Structures of germanium clusters: where the growth patterns of silicon and germanium clusters diverge. *Phys. Rev. Lett.* **83**, 2167–2170 (1999). <https://doi.org/10.1103/PhysRevLett.83.2167>
58. O. Cheshnovsky, S.H. Yang, C.L. Pettiette, M.J. Craycraft, Y. Liu, R.E. Smalley, Ultraviolet photoelectron spectroscopy of semiconductor clusters: silicon and germanium. *Chem. Phys. Lett.* **138**(2), 119–124 (1987). [https://doi.org/10.1016/0009-2614\(87\)80353-6](https://doi.org/10.1016/0009-2614(87)80353-6)
59. G. Ganteför, M. Gausa, K.-H. Meiwes-Broer, H.O. Lutz, Photoemission from tin and lead cluster anions. *Z. Phys. D* **12**(1), 405–409 (1989). <https://doi.org/10.1007/BF01426983>